

000 054  
 001 055  
 002 056  
 003 057  
 004 058  
 005 059  
 006 060  
 007 061  
 008 062  
 009 063  
 010 064  
 011 065  
 012 066  
 013 067  
 014 068  
 015 069  
 016 070  
 017 071  
 018 072  
 019 073  
 020 074  
 021 075  
 022 076  
 023 077  
 024 078  
 025 079  
 026 080  
 027 081  
 028 082  
 029 083  
 030 084  
 031 085  
 032 086  
 033 087  
 034 088  
 035 089  
 036 090  
 037 091  
 038 092  
 039 093  
 040 094  
 041 095  
 042 096  
 043 097  
 044 098  
 045 099  
 046 100  
 047 101  
 048 102  
 049 103  
 050 104  
 051 105  
 052 106  
 053 107

## Supplementary Materials to ‘‘Multi-channel Weighted Nuclear Norm Minimization for Real Color Image Denoising’’

Anonymous ICCV submission

Paper ID 572

In this supplementary file, we provide:

1. The proof of the Theorem 1 in the main paper;
2. More denoising results on the Kodak PhotoCD dataset;
3. More visual comparisons of denoised images on the real noisy images of dataset [1];
4. More visual comparisons of denoised images on the real noisy images of dataset [2].

### 1. Proof of Theorem 1.

**Theorem 1.** Assume that the weights in  $w$  are in a non-descending order, the sequence  $\{\mathbf{X}_k\}$ ,  $\{\mathbf{Z}_k\}$ , and  $\{\mathbf{A}_k\}$  generated in Algorithm 1 satisfy:

$$(a) \lim_{k \rightarrow \infty} \|\mathbf{X}_{k+1} - \mathbf{Z}_{k+1}\|_F = 0; \quad (b) \lim_{k \rightarrow \infty} \|\mathbf{X}_{k+1} - \mathbf{X}_k\|_F = 0; \quad (c) \lim_{k \rightarrow \infty} \|\mathbf{Z}_{k+1} - \mathbf{Z}_k\|_F = 0. \quad (1)$$

*Proof.* 1. Firstly, we prove that the sequence  $\{\mathbf{A}_k\}$  generated by Algorithm 1 is upper bounded. Let  $\mathbf{X}_{k+1} + \rho_k^{-1} \mathbf{A}_k = \mathbf{U}_k \Sigma_k \mathbf{V}_k^\top$  be its singular value decomposition (SVD) [3] in the  $(k+1)$ -th iteration. According to Corollary 1 of [4], we can have the SVD of  $\mathbf{Z}_{k+1}$  as  $\mathbf{Z}_{k+1} = \mathbf{U}_k \hat{\Sigma}_k \mathbf{V}_k^\top = \mathbf{U}_k \mathcal{S}_{\frac{w}{\rho_k}}(\Sigma_k) \mathbf{V}_k^\top$ . Then we have

$$\|\mathbf{A}_{k+1}\|_F = \|\mathbf{A}_k + \rho_k(\mathbf{X}_{k+1} - \mathbf{Z}_{k+1})\|_F = \rho_k \|\rho_k^{-1} \mathbf{A}_k + \mathbf{X}_{k+1} - \mathbf{Z}_{k+1}\|_F \quad (2)$$

$$= \rho_k \|\mathbf{U}_k \Sigma_k \mathbf{V}_k^\top - \mathbf{U}_k \mathcal{S}_{\frac{w}{\rho_k}}(\Sigma_k) \mathbf{V}_k^\top\|_F = \rho_k \|\Sigma_k - \mathcal{S}_{\frac{w}{\rho_k}}(\Sigma_k)\|_F \quad (3)$$

$$= \rho_k \sqrt{\sum_i (\Sigma_k^{ii} - \mathcal{S}_{\frac{w}{\rho_k}}(\Sigma_k^{ii}))^2} \leq \rho_k \sqrt{\sum_i (\frac{w_i}{\rho_k})^2} = \sqrt{\sum_i w_i^2}. \quad (4)$$

The inequality in the second last step can be proved as follows: given the diagonal matrix  $\Sigma_k$ , we define  $\Sigma_k^{ii}$  as the  $i$ -th element of  $\Sigma_k^{ii}$ . If  $\Sigma_k^{ii} \geq \frac{w_i}{\rho_k}$ , we have  $\mathcal{S}_{\frac{w}{\rho_k}}(\Sigma_k^{ii}) = \Sigma_k^{ii} - \frac{w_i}{\rho_k}$ . If  $\Sigma_k^{ii} < \frac{w_i}{\rho_k}$ , we have  $\mathcal{S}_{\frac{w}{\rho_k}}(\Sigma_k^{ii}) = 0$ . Overall, we have  $|\Sigma_k^{ii} - \mathcal{S}_{\frac{w}{\rho_k}}(\Sigma_k^{ii})| \leq \frac{w_i}{\rho_k}$  and hence the inequality holds. Hence, the sequence  $\{\mathbf{A}_k\}$  is upper bounded.

2. Secondly, we prove that the sequence of Lagrangian function  $\{\mathcal{L}(\mathbf{X}_{k+1}, \mathbf{Z}_{k+1}, \mathbf{A}_k, \rho_k)\}$  is also upper bounded. Since we have the globally optimal solution of  $\mathbf{X}$  and  $\mathbf{Z}$  in their corresponding subproblems, we always have

$$\mathcal{L}(\mathbf{X}_{k+1}, \mathbf{Z}_{k+1}, \mathbf{A}_k, \rho_k) \leq \mathcal{L}(\mathbf{X}_k, \mathbf{Z}_k, \mathbf{A}_k, \rho_k). \quad (5)$$

Based on the updating rule that  $\mathbf{A}_{k+1} = \mathbf{A}_k + \rho_k(\mathbf{X}_{k+1} - \mathbf{Z}_{k+1})$ , we have

$$\mathcal{L}(\mathbf{X}_{k+1}, \mathbf{Z}_{k+1}, \mathbf{A}_{k+1}, \rho_{k+1}) \quad (6)$$

$$= \mathcal{L}(\mathbf{X}_{k+1}, \mathbf{Z}_{k+1}, \mathbf{A}_k, \rho_k) + \langle \mathbf{A}_{k+1} - \mathbf{A}_k, \mathbf{X}_{k+1} - \mathbf{Z}_{k+1} \rangle + \frac{\rho_{k+1} - \rho_k}{2} \|\mathbf{X}_{k+1} - \mathbf{Z}_{k+1}\|_F^2 \quad (7)$$

$$= \mathcal{L}(\mathbf{X}_{k+1}, \mathbf{Z}_{k+1}, \mathbf{A}_k, \rho_k) + \frac{\rho_{k+1} + \rho_k}{2\rho_k^2} \|\mathbf{A}_{k+1} - \mathbf{A}_k\|_F^2. \quad (8)$$

108 Since the sequence  $\{\|\mathbf{A}_k\|\}$  is upper bounded, the sequence  $\{\|\mathbf{A}_{k+1} - \mathbf{A}_k\|_F\}$  is also upper bounded. Denote by  $a$  the upper  
109 bound of  $\{\|\mathbf{A}_{k+1} - \mathbf{A}_k\|_F\}$ , we have  
110

$$\begin{aligned} 111 \quad \mathcal{L}(\mathbf{X}_{k+1}, \mathbf{Z}_{k+1}, \mathbf{A}_{k+1}, \rho_{k+1}) &\leq \mathcal{L}(\mathbf{X}_1, \mathbf{Z}_1, \mathbf{A}_0, \rho_0) + a \sum_{k=0}^{\infty} \frac{\rho_{k+1} + \rho_k}{2\rho_k^2} \\ 112 \end{aligned} \quad (9)$$

$$\begin{aligned} 113 \quad &= \mathcal{L}(\mathbf{X}_1, \mathbf{Z}_1, \mathbf{A}_0, \rho_0) + a \sum_{k=0}^{\infty} \frac{\mu + 1}{2\mu^k \rho_0} \\ 114 \end{aligned} \quad (10)$$

$$\begin{aligned} 115 \quad &\leq \mathcal{L}(\mathbf{X}_1, \mathbf{Z}_1, \mathbf{A}_0, \rho_0) + \frac{a}{\rho_0} \sum_{k=0}^{\infty} \frac{1}{\mu^{k-1}}. \\ 116 \end{aligned} \quad (11)$$

117 The last inequality holds since  $\mu > 1$  and  $\mu + 1 < 2\mu$ . Therefore, we have  $\sum_{k=0}^{\infty} \frac{1}{\mu^{k-1}} < \infty$  and the sequence of Lagrangian  
118 function  $\{\mathcal{L}(\mathbf{X}_{k+1}, \mathbf{Z}_{k+1}, \mathbf{A}_{k+1}, \rho_{k+1})\}$  is upper bound.  
119

120 3. Thirdly, we prove that the sequences of  $\{\mathbf{X}_k\}$  and  $\{\mathbf{Z}_k\}$  are upper bounded. Since  
121

$$\begin{aligned} 122 \quad \|\mathbf{W}(\mathbf{Y} - \mathbf{X}_k)\|_F^2 + \|\mathbf{Z}_k\|_{\mathbf{w},*}^2 &= \mathcal{L}(\mathbf{X}_k, \mathbf{Z}_k, \mathbf{A}_{k-1}, \rho_{k-1}) - \langle \mathbf{A}_k, \mathbf{X}_k - \mathbf{Z}_k \rangle - \frac{\rho_k}{2} \|\mathbf{X}_k - \mathbf{Z}_k\|_F^2 \\ 123 \end{aligned} \quad (12)$$

$$\begin{aligned} 124 \quad &= \mathcal{L}(\mathbf{X}_k, \mathbf{Z}_k, \mathbf{A}_{k-1}, \rho_{k-1}) + \frac{1}{2\rho_k} (\|\mathbf{A}_{k-1}\|_F^2 - \|\mathbf{A}_k\|_F^2), \\ 125 \end{aligned} \quad (13)$$

126 both  $\{\mathbf{W}(\mathbf{Y} - \mathbf{X}_k)\}$  and  $\{\mathbf{Z}_k\}$  are upper bounded, and hence the sequence  $\{\mathbf{X}_k\}$  is bounded by the Cauchy-Schwarz  
127 inequality and triangle inequality. We can obtain that  
128

$$\lim_{k \rightarrow \infty} \|\mathbf{X}_{k+1} - \mathbf{Z}_{k+1}\|_F = \lim_{k \rightarrow \infty} \rho_k^{-1} \|\mathbf{A}_{k+1} - \mathbf{A}_k\|_F = 0, \quad (14)$$

129 and the equation (a) is proved.  
130

131 4. Then we can prove that

$$\begin{aligned} 132 \quad \lim_{k \rightarrow \infty} \|\mathbf{X}_{k+1} - \mathbf{X}_k\|_F &= \lim_{k \rightarrow \infty} \|(\mathbf{W}^\top \mathbf{W} + \frac{\rho_k}{2} \mathbf{I})^{-1} (\mathbf{W}^\top \mathbf{W} \mathbf{Y} - \mathbf{W}^\top \mathbf{W} \mathbf{Z}_k - \frac{1}{2} \mathbf{A}_k) - \rho_k^{-1} (\mathbf{A}_k - \mathbf{A}_{k-1})\|_F \\ 133 \end{aligned} \quad (15)$$

$$\begin{aligned} 134 \quad &\leq \lim_{k \rightarrow \infty} \|(\mathbf{W}^\top \mathbf{W} + \frac{\rho_k}{2} \mathbf{I})^{-1} (\mathbf{W}^\top \mathbf{W} \mathbf{Y} - \mathbf{W}^\top \mathbf{W} \mathbf{Z}_k - \frac{1}{2} \mathbf{A}_k)\|_F + \rho_k^{-1} \|\mathbf{A}_k - \mathbf{A}_{k-1}\|_F \\ 135 \end{aligned} \quad (16)$$

$$136 \quad = 0, \quad (17)$$

137 and hence the equation (b) is proved.  
138

139 5. Finally, the equation (c) can be proved by checking that

$$\begin{aligned} 140 \quad \lim_{k \rightarrow \infty} \|\mathbf{Z}_{k+1} - \mathbf{Z}_k\|_F &= \lim_{k \rightarrow \infty} \|\mathbf{X}_k + \rho_k^{-1} \mathbf{A}_{k-1} - \mathbf{Z}_k + \mathbf{X}_{k+1} - \mathbf{X}_k + \rho_k^{-1} \mathbf{A}_{k-1} + \rho_k^{-1} \mathbf{A}_k - \rho_k^{-1} \mathbf{A}_{k+1}\|_F \\ 141 \end{aligned} \quad (18)$$

$$\begin{aligned} 142 \quad &\leq \lim_{k \rightarrow \infty} \|\Sigma_{k-1} - \mathcal{S}_{\mathbf{w}/\rho_{k-1}}(\Sigma_{k-1})\|_F + \|\mathbf{X}_{k+1} - \mathbf{X}_k\|_F + \rho_k^{-1} \|\mathbf{A}_{k-1} + \mathbf{A}_{k+1} - \mathbf{A}_k\|_F \\ 143 \end{aligned} \quad (19)$$

$$\begin{aligned} 144 \quad &\leq \lim_{k \rightarrow \infty} \rho_{k-1}^{-1} \|\mathbf{w}\|_F + \|\mathbf{X}_{k+1} - \mathbf{X}_k\|_F + \rho_k^{-1} \|\mathbf{A}_{k-1} + \mathbf{A}_{k+1} - \mathbf{A}_k\|_F \\ 145 \end{aligned} \quad (20)$$

$$146 \quad = 0, \quad (21)$$

147 where  $\mathbf{U}_{k-1} \Sigma_{k-1} \mathbf{V}_{k-1}^\top$  is the SVD of the matrix  $\mathbf{X}_k + \rho_{k-1} \mathbf{A}_{k-1}$ .  
148

## 149 2. More denoising results on the Kodak PhotoCD dataset

150 In the main paper, we have given the PSNR results of the competing methods on the 24 high quality images from the  
151 Kodak PhotoCD dataset when the standard deviations of the additive white Gaussian noise (AWGN) are  $\sigma_r = 40, \sigma_g = 20, \sigma_b = 30$  for R, G, B channels, respectively. Here we provide more denoising results on this dataset. In Tables 1-3,  
152 we give the PSNR results on these images when the noise standard deviations are  $\sigma_r = 40, \sigma_g = 20, \sigma_b = 30$  in Table 1,  
153  $\sigma_r = 30, \sigma_g = 10, \sigma_b = 50$  in Table 2 and  $\sigma_r = 5, \sigma_g = 30, \sigma_b = 15$  in Table 3, respectively. In Figures 1-6, we give the  
154 visual comparisons of the denoised images by different methods.  
155

Table 1. PSNR(dB) results of different denoising methods on the Kodak PhotoCD dataset.

Image#	$\sigma_r = 40, \sigma_g = 20, \sigma_b = 30$								
	CBM3D	MLP	TNRD	NI	NC	WNNM-1	WNNM-2	WNNM-3	MC-WNNM
1	25.24	25.70	25.74	23.85	24.90	26.01	25.95	25.58	<b>26.66</b>
2	28.27	30.12	30.21	25.90	25.87	30.08	30.11	29.80	<b>30.20</b>
3	28.81	31.19	31.49	26.00	28.58	31.58	31.61	31.20	<b>32.25</b>
4	27.95	29.88	29.86	25.82	25.67	30.13	30.16	29.84	<b>30.49</b>
5	25.03	26.00	26.18	24.38	25.15	26.44	26.39	25.32	<b>26.82</b>
6	26.24	26.84	26.90	24.65	24.74	27.39	27.30	26.88	<b>27.98</b>
7	27.88	30.28	30.40	25.63	27.69	30.47	30.54	29.70	<b>30.98</b>
8	25.05	25.59	25.83	24.02	25.30	26.71	26.75	25.26	<b>26.90</b>
9	28.44	30.75	30.81	25.94	27.44	30.86	30.92	30.29	<b>31.49</b>
10	28.27	30.38	30.57	25.87	28.42	30.65	30.68	29.95	<b>31.26</b>
11	26.95	28.00	28.14	25.32	24.67	28.19	28.16	27.61	<b>28.63</b>
12	28.76	30.87	31.05	26.01	28.37	30.97	31.06	30.58	<b>31.48</b>
13	23.76	23.95	23.99	23.53	22.76	24.27	24.15	23.52	<b>24.89</b>
14	26.02	26.97	27.11	24.94	25.68	27.20	27.15	26.55	<b>27.57</b>
15	28.38	30.15	30.44	26.06	28.21	30.52	30.60	30.13	<b>30.81</b>
16	27.75	28.82	28.87	25.69	26.66	29.27	29.21	29.02	<b>29.96</b>
17	27.90	29.57	29.80	25.85	28.32	29.78	29.79	29.16	<b>30.40</b>
18	25.77	26.40	26.41	24.74	25.70	26.63	26.56	26.01	<b>27.22</b>
19	27.30	28.67	28.81	25.40	26.52	29.19	29.22	28.67	<b>29.57</b>
20	28.96	30.40	30.76	24.95	25.90	30.79	30.83	29.97	<b>31.07</b>
21	26.54	27.53	27.60	25.06	26.48	27.80	27.75	27.12	<b>28.34</b>
22	27.05	28.17	28.27	25.36	26.60	28.21	28.16	27.81	<b>28.64</b>
23	29.14	32.31	32.51	26.13	23.24	31.89	31.97	31.21	<b>32.34</b>
24	25.75	26.41	26.53	24.55	25.73	27.10	27.03	26.18	<b>27.59</b>
<b>Average</b>	27.13	28.54	28.68	25.24	26.19	28.84	28.83	28.22	<b>29.31</b>

Table 2. PSNR(dB) results of different denoising methods on the Kodak PhotoCD dataset.

Image#	$\sigma_r = 30, \sigma_g = 10, \sigma_b = 50$								
	CBM3D	MLP	TNRD	NI	NC	WNNM-1	WNNM-2	WNNM-3	MC-WNNM
1	23.38	26.49	26.50	24.82	23.59	26.40	25.60	24.76	<b>27.81</b>
2	25.19	30.94	30.90	26.82	27.79	30.89	29.75	29.21	<b>30.96</b>
3	25.39	32.03	32.09	27.52	27.41	32.20	31.17	30.39	<b>32.89</b>
4	24.96	30.55	30.47	27.34	27.00	30.74	29.71	29.10	<b>31.19</b>
5	23.29	26.65	26.73	25.72	26.67	26.74	25.98	24.68	<b>27.60</b>
6	24.09	27.76	27.70	26.10	26.12	27.85	26.96	26.01	<b>29.15</b>
7	24.89	30.70	30.72	27.17	28.07	30.91	29.94	28.87	<b>31.37</b>
8	23.30	26.12	26.27	25.59	26.11	26.87	26.33	24.74	<b>27.44</b>
9	25.20	31.35	31.31	27.74	28.33	31.30	30.45	29.44	<b>32.08</b>
10	25.13	31.01	31.05	27.60	28.53	31.12	30.17	29.21	<b>31.83</b>
11	24.54	28.79	28.82	26.72	24.40	28.73	27.79	26.94	<b>29.60</b>
12	25.43	31.60	31.60	27.82	29.01	31.59	30.62	29.91	<b>32.11</b>
13	22.50	24.71	24.73	24.96	23.36	24.70	23.85	22.86	<b>25.96</b>
14	23.91	27.69	27.72	26.26	23.08	27.62	26.81	25.91	<b>28.57</b>
15	25.45	31.09	31.05	27.36	28.49	31.29	30.21	29.46	<b>31.39</b>
16	24.89	29.79	29.73	27.35	27.10	29.84	28.85	28.13	<b>31.10</b>
17	25.12	30.26	30.24	27.15	27.54	30.11	29.35	28.43	<b>31.08</b>
18	23.83	27.26	27.26	26.05	26.15	27.32	26.18	25.28	<b>28.32</b>
19	24.63	29.40	29.39	27.06	27.41	29.78	28.87	28.05	<b>30.53</b>
20	26.43	31.16	31.27	26.43	26.92	31.25	30.43	29.41	<b>31.55</b>
21	24.24	28.26	28.27	26.66	27.18	28.22	27.45	26.40	<b>29.29</b>
22	24.51	29.03	29.06	26.83	27.64	29.02	27.81	27.18	<b>29.57</b>
23	25.55	32.87	32.75	27.60	23.75	32.58	31.46	30.50	<b>32.34</b>
24	23.85	27.06	27.13	25.86	27.05	27.50	26.63	25.55	<b>28.32</b>
<b>Average</b>	24.57	29.27	29.28	26.69	26.61	29.36	28.43	27.52	<b>30.09</b>

324 Table 3. PSNR(dB) results of different denoising methods on the Kodak PhotoCD dataset. 378  
325  $\sigma_r = 5, \sigma_g = 30, \sigma_b = 15$  379

Image#	CBM3D	MLP	TNRD	NI	NC	WNNM-1	WNNM-2	WNNM-3	MC-WNNM
1	27.25	28.06	28.62	25.00	29.55	28.16	27.95	28.15	<b>30.20</b>
2	29.70	31.30	32.70	27.80	29.69	32.54	31.60	31.73	<b>34.04</b>
3	30.34	31.98	34.07	28.02	31.93	33.91	33.68	33.52	<b>35.55</b>
4	29.47	31.10	32.56	27.70	32.56	32.68	31.85	31.90	<b>34.06</b>
5	27.31	28.59	29.35	26.14	30.00	28.83	29.00	28.91	<b>30.05</b>
6	28.20	29.10	29.90	26.15	28.81	29.55	29.46	29.62	<b>31.64</b>
7	29.73	31.60	33.46	27.22	31.63	33.09	33.29	32.86	<b>34.24</b>
8	27.47	28.16	28.91	25.34	30.16	29.15	29.24	29.03	<b>29.91</b>
9	30.07	31.63	33.55	27.86	31.54	33.19	33.20	32.95	<b>34.53</b>
10	29.96	31.37	33.20	27.74	33.44	32.98	33.02	32.74	<b>34.38</b>
11	28.73	29.85	30.87	26.98	30.16	30.45	30.14	30.21	<b>32.10</b>
12	30.20	31.50	33.31	27.97	31.69	33.22	32.71	32.65	<b>34.64</b>
13	26.18	26.69	26.98	25.14	27.97	26.49	26.42	26.62	<b>28.30</b>
14	27.86	29.07	29.87	26.67	29.21	29.36	29.14	29.30	<b>31.18</b>
15	29.91	31.58	33.13	28.04	31.17	33.22	32.34	32.36	<b>34.27</b>
16	29.29	30.35	31.54	27.46	32.18	31.34	31.05	31.21	<b>33.72</b>
17	29.50	31.09	32.52	27.81	32.80	32.09	32.00	31.85	<b>33.61</b>
18	27.72	28.74	29.36	26.57	28.63	28.88	28.76	28.89	<b>30.56</b>
19	28.98	30.18	31.35	27.25	29.79	31.34	30.77	30.95	<b>33.10</b>
20	30.63	31.78	33.27	27.89	29.52	33.00	32.55	32.58	<b>34.18</b>
21	28.50	29.58	30.54	26.86	30.99	30.02	30.03	30.03	<b>31.69</b>
22	28.61	29.78	30.82	27.19	30.50	30.47	29.82	30.10	<b>32.08</b>
23	30.60	32.66	35.06	28.17	32.82	34.72	34.37	33.94	<b>35.16</b>
24	27.97	28.81	29.61	26.01	30.75	29.47	29.35	29.39	<b>30.93</b>
Average	28.92	30.19	31.44	27.04	30.73	31.17	30.91	30.89	<b>32.67</b>

350 

### 3. More visual comparisons of denoised images on the real noisy images of dataset [1]

 404  
351

In this section, we give more comparisons of the state-of-the-art denoising methods on dataset [1]. The real noisy images in dataset [1] have no “ground truth” images and hence we only compare the visual quality of the denoised images by different methods. As can be seen from Figures 7-10, the proposed MC-WNNM method performs better than the competing methods.

355 

### 4. More visual comparisons of denoised images on the real noisy images of dataset [2]

 409  
356

In this section, we provide more comparisons of the proposed method with the state-of-the-art denoising methods on the 15 cropped real noisy images used in [2]. In this dataset, each scene was shot 500 times under the same camera and camera setting. The mean image of the 500 shots is roughly taken as the “ground truth”, with which the PSNR can be computed. As can be seen from Figures 11-14, in most cases, our proposed method achieves better performance than the the competing methods. This validates the effectiveness of the proposed MC-WNNM method for real noisy image denoising.

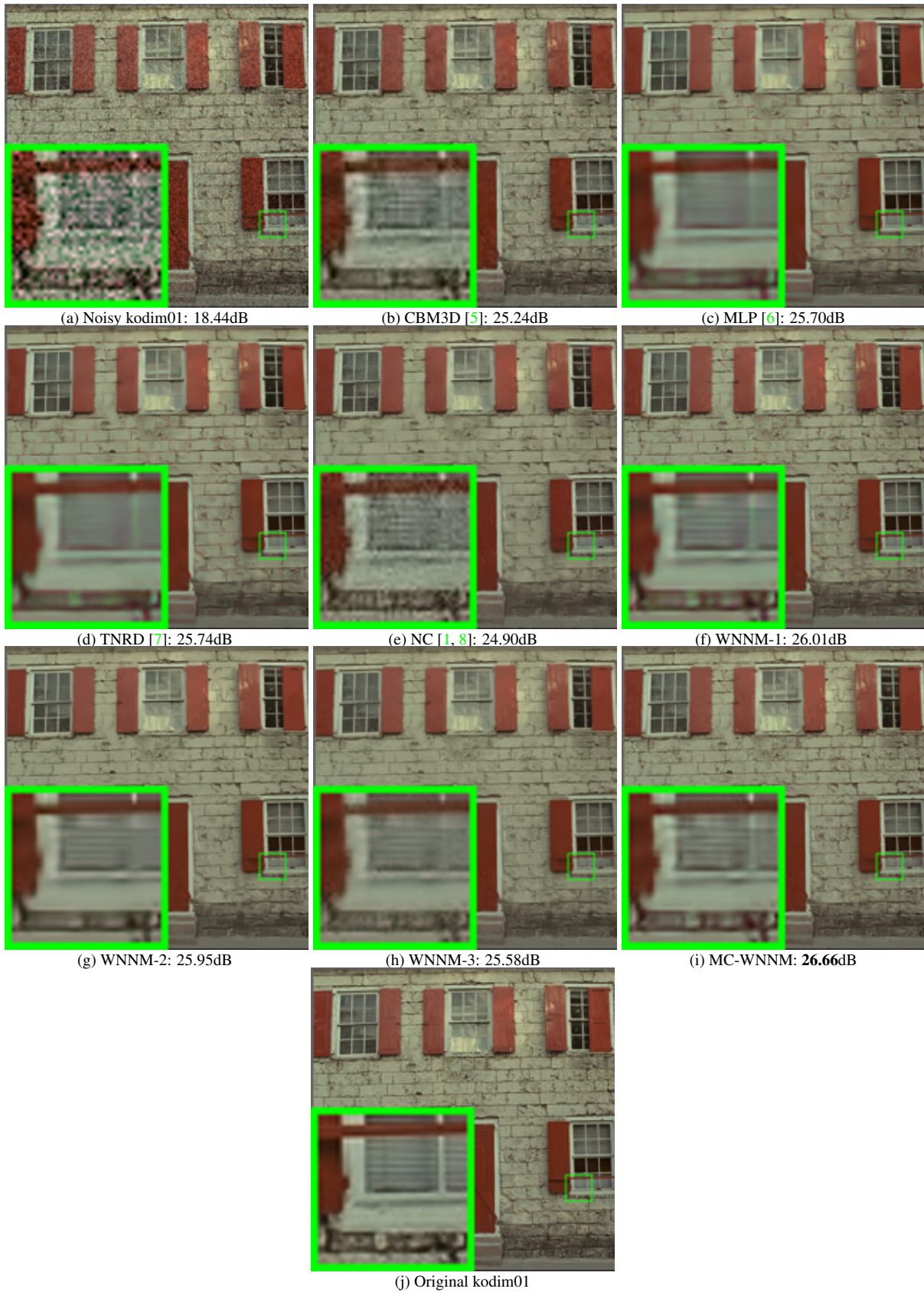


Figure 1. Denoised images of different methods on the image "kodim01" degraded by AWGN with different standard deviations of  $\sigma_r = 40$ ,  $\sigma_g = 20$ ,  $\sigma_b = 30$  on R, G, B channels, respectively. The images are better to be zoomed in on screen.

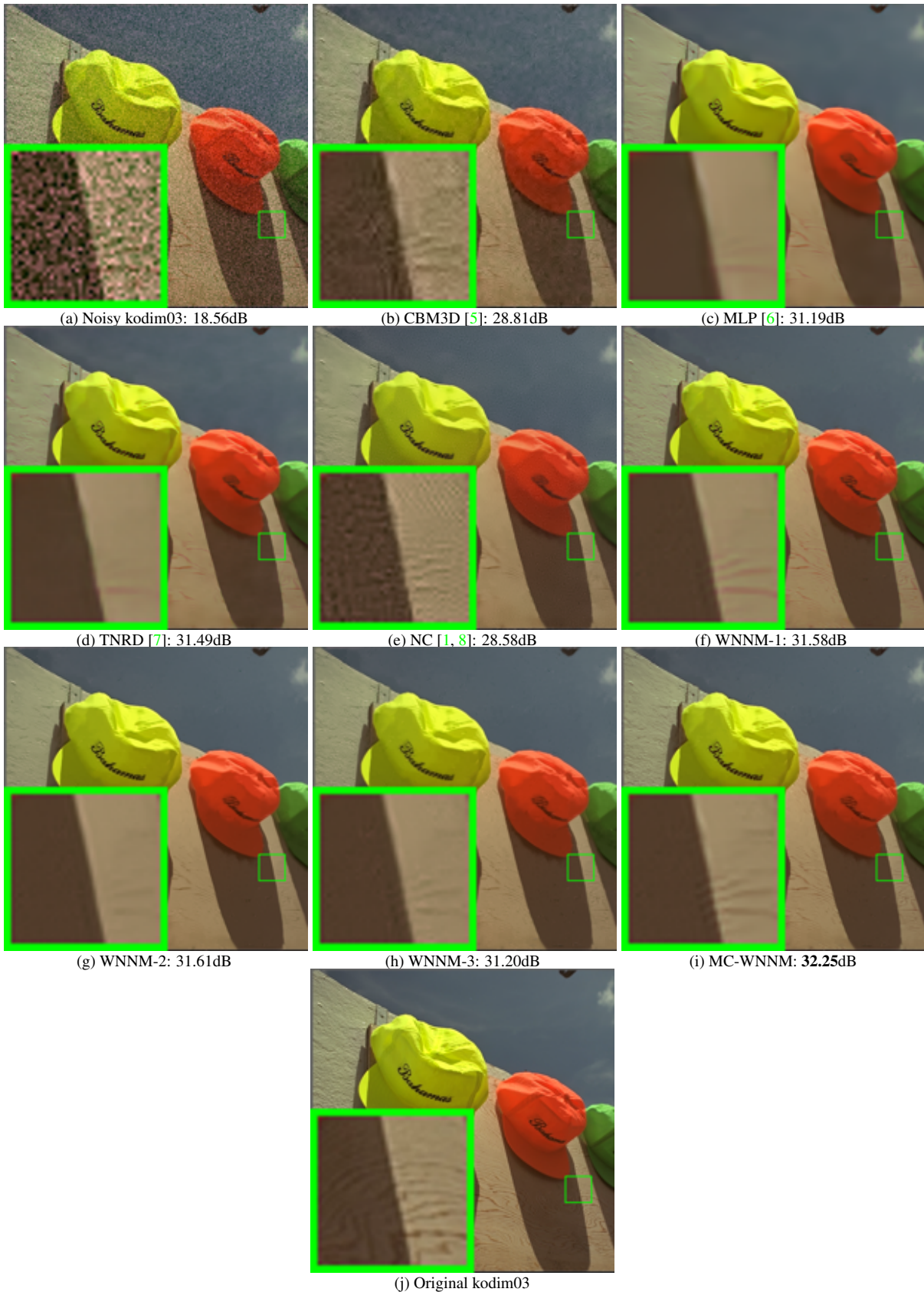


Figure 2. Denoised images of different methods on the image "kodim03" degraded by AWGN with different standard deviations of  $\sigma_r = 40$ ,  $\sigma_g = 20$ ,  $\sigma_b = 30$  on R, G, B channels, respectively. The images are better to be zoomed in on screen.

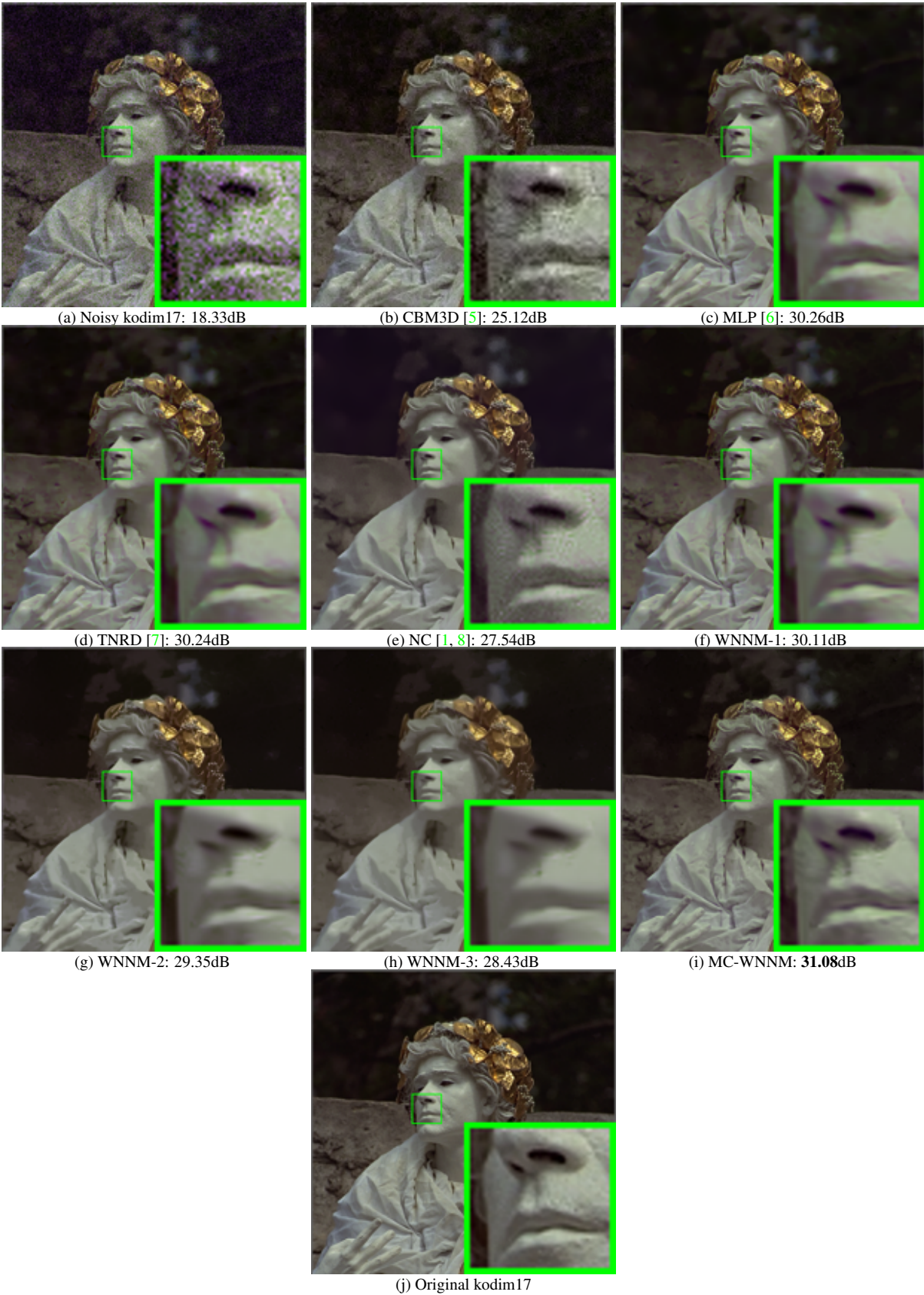


Figure 3. Denoised images of different methods on the image "kodim17" degraded by AWGN with different standard deviations of  $\sigma_r = 30$ ,  $\sigma_g = 10$ ,  $\sigma_b = 50$  on R, G, B channels, respectively. The images are better to be zoomed in on screen.

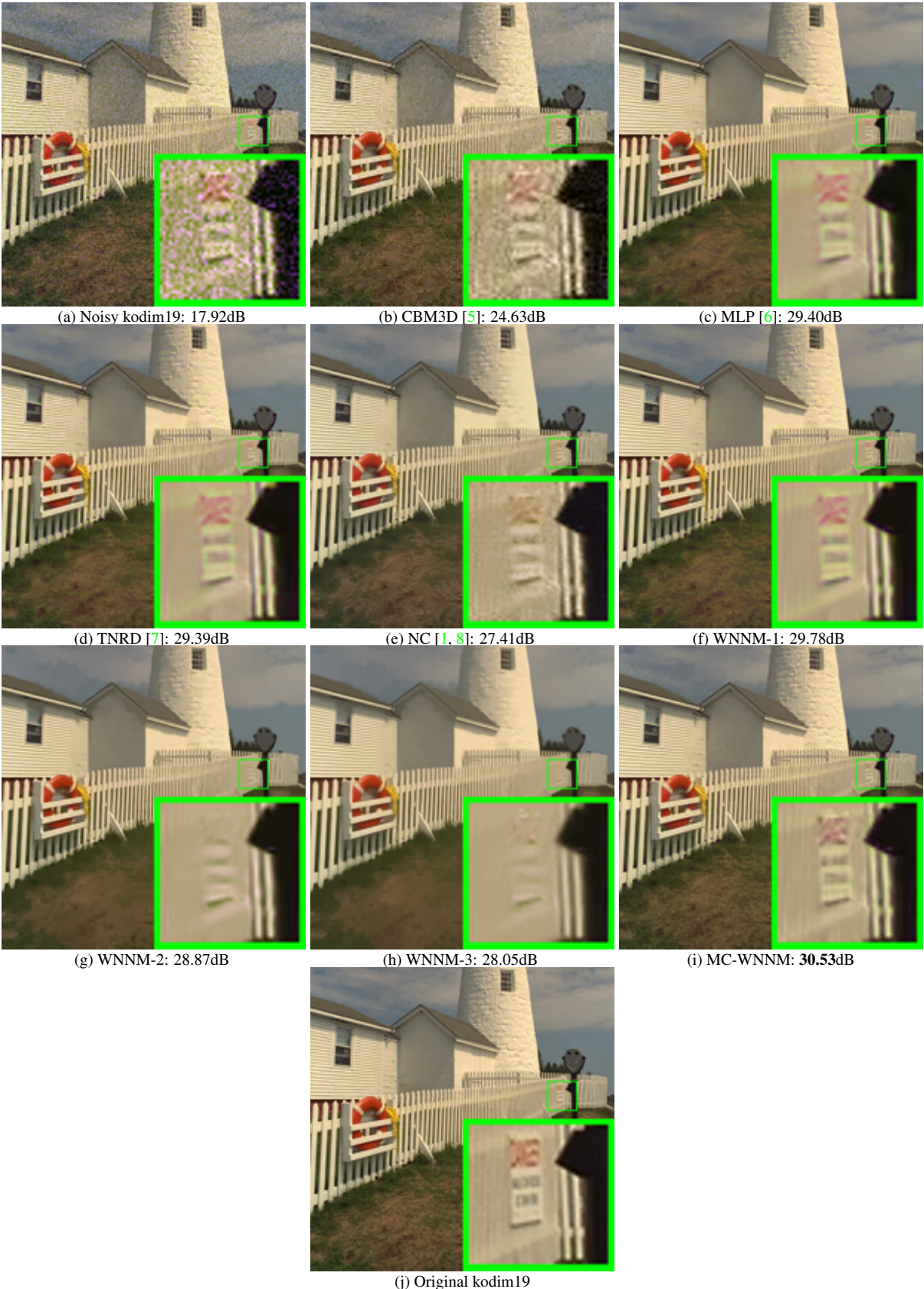
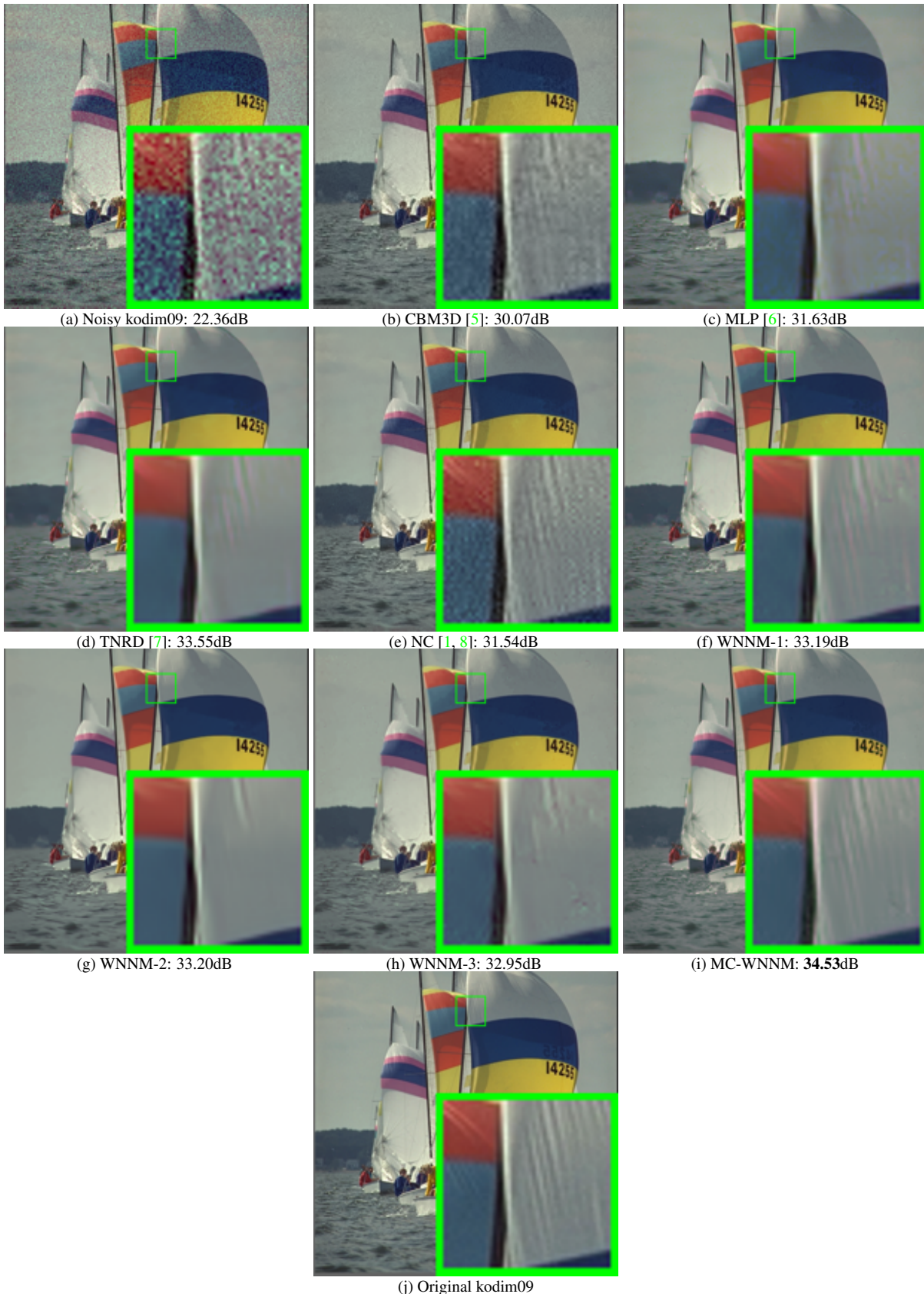


Figure 4. Denoised images of different methods on the image "kodim19" degraded by AWGN with different standard deviations of  $\sigma_r = 30$ ,  $\sigma_g = 10$ ,  $\sigma_b = 50$  on R, G, B channels, respectively. The images are better to be zoomed in on screen.



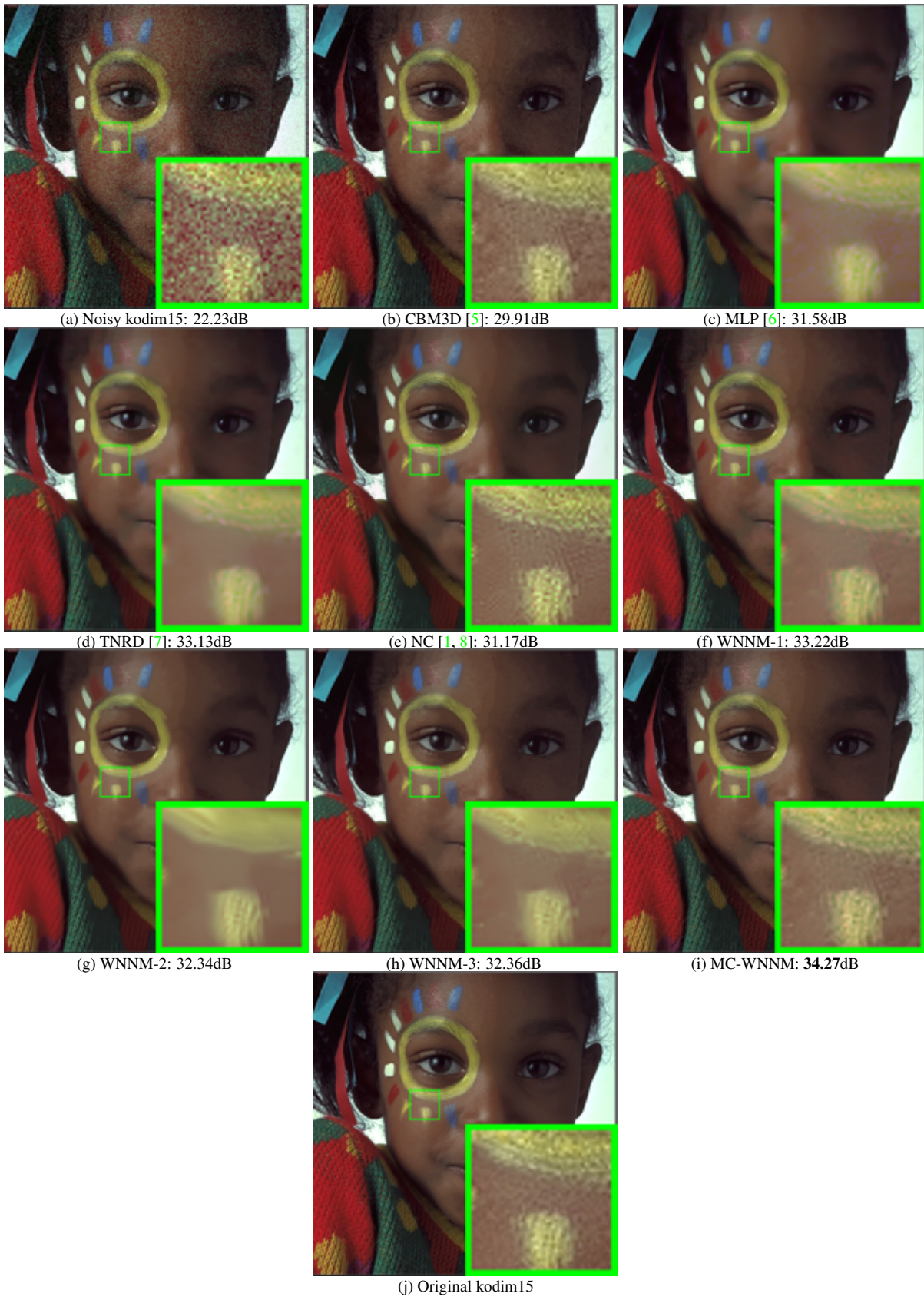


Figure 6. Denoised images of different methods on the image "kodim15" degraded by AWGN with different standard deviations of  $\sigma_r = 5, \sigma_g = 30, \sigma_b = 15$  on R, G, B channels, respectively. The images are better to be zoomed in on screen.

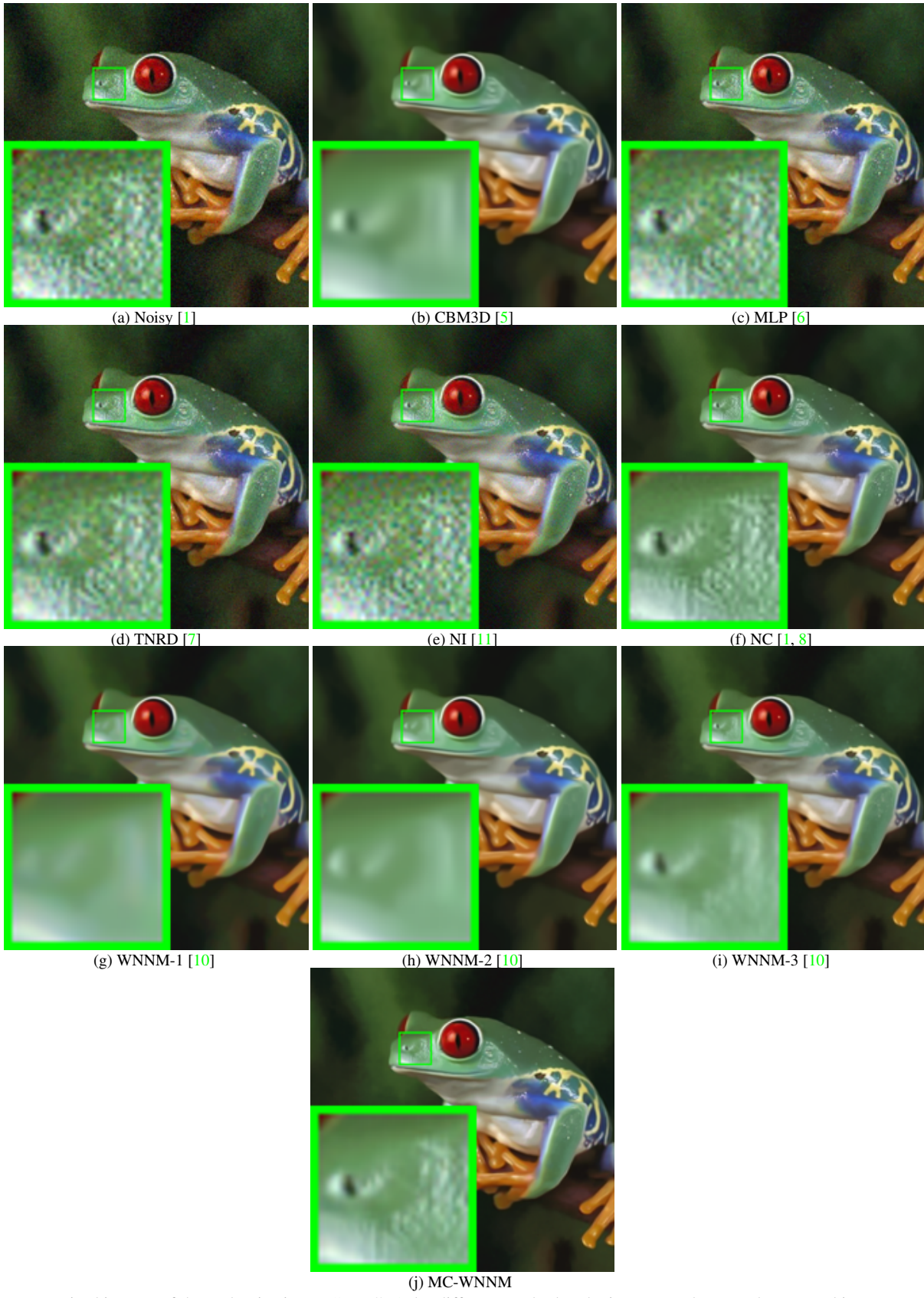


Figure 7. Denoised images of the real noisy image "Frog" [1] by different methods. The images are better to be zoomed in on screen.

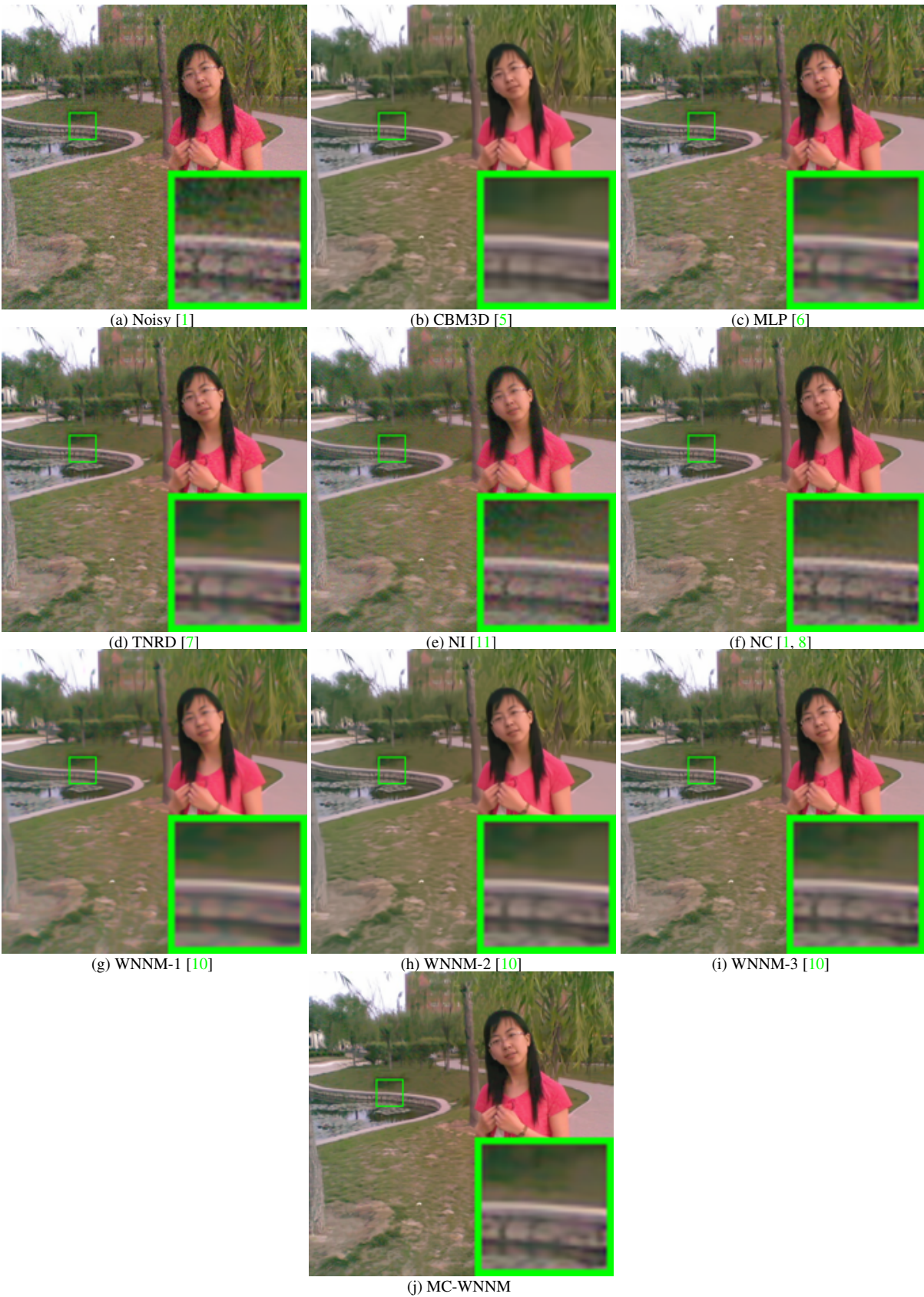
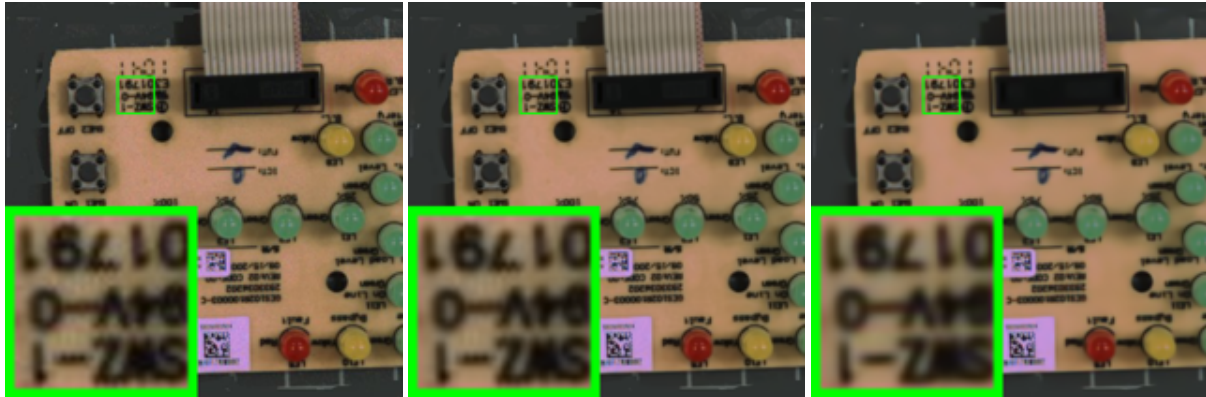


Figure 8. Denoised images of the real noisy image "Gril" [1] by different methods. The images are better to be zoomed in on screen.

1296  
1297  
1298  
1299  
1300  
1301  
1302  
1303  
1304  
1305  
1306  
1307  
1308

(a) Noisy [1]

(b) CBM3D [5]

(c) MLP [6]

(d) TNRD [7]

(e) NI [11]

(f) NC [1, 8]

(g) WNNM-1 [10]

(h) WNNM-2 [10]

(i) WNNM-3 [10]

Figure 9. Denoised images of the real noisy image “Circuit” [1] by different methods. The images are better to be zoomed on screen.

1349

1350  
1351  
1352  
1353  
1354  
1355  
1356  
1357  
1358  
1359  
1360  
1361  
1362  
1363  
1364  
1365  
1366  
1367  
1368  
1369  
1370  
1371  
1372  
1373  
1374  
1375  
1376  
1377  
1378  
1379  
1380  
1381  
1382  
1383  
1384  
1385  
1386  
1387  
1388  
1389  
1390  
1391  
1392  
1393  
1394  
1395  
1396  
1397  
1398  
1399  
1400  
1401  
1402  
1403

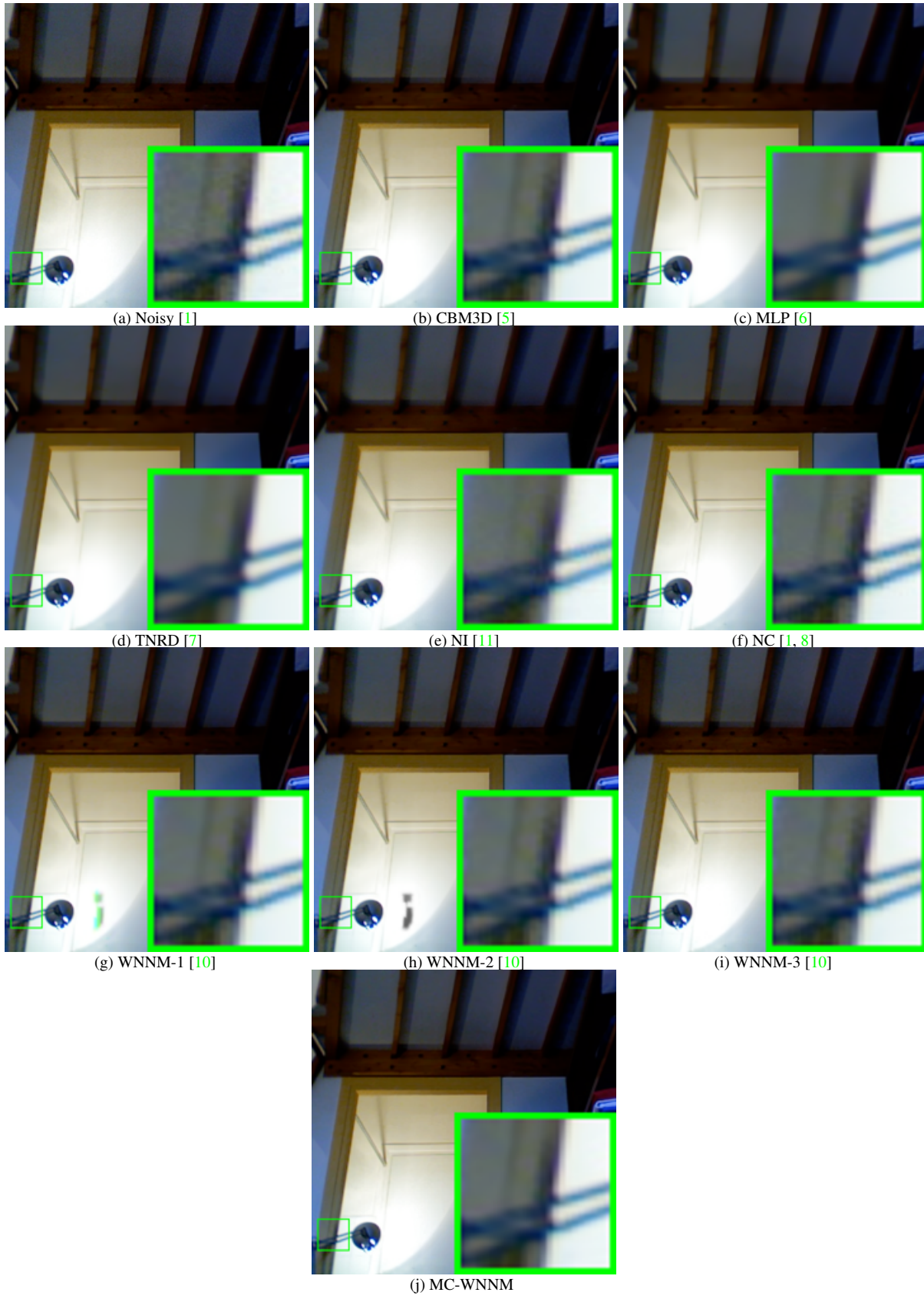
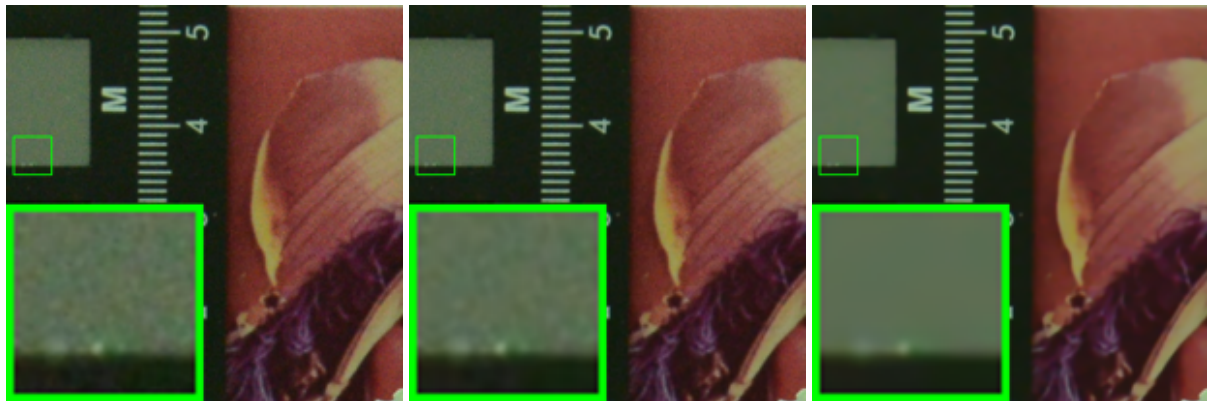


Figure 10. Denoised images of the real noisy image “Room” [1] by different methods. The images are better to be zoomed in on screen.



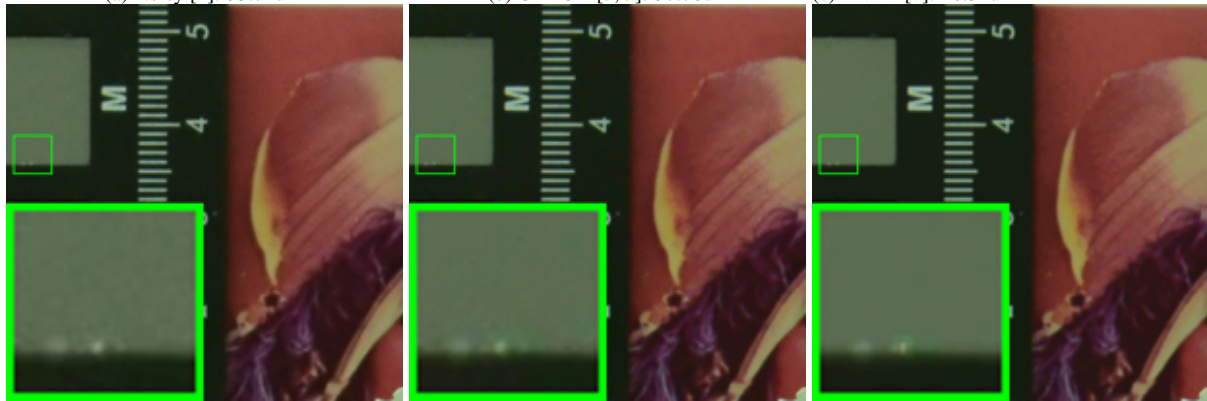
Figure 11. Denoised images of a region cropped from the real noisy image “Nikon D600 ISO 3200 2” [2] by different methods. The images are better to be zoomed in on screen.

1620  
1621  
1622  
1623  
1624  
1625  
1626  
1627  
1628  
1629  
1630  
1631

(a) Noisy [2]: 35.71dB

(b) CBM3D [5, 9]: 37.76dB

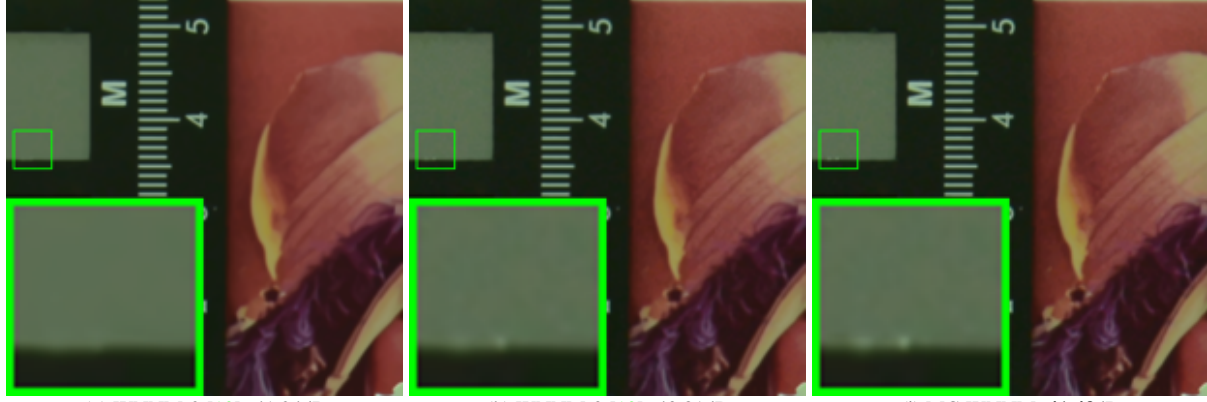
(c) TNRD [7]: 40.52dB

1632  
1633  
1634  
1635  
1636  
1637  
1638  
1639  
1640  
1641  
1642  
1643  
1644  
1645

(d) NI [11]: 38.42dB

(e) NC [1, 8]: 38.65dB

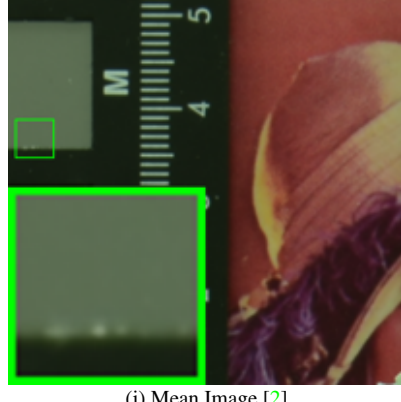
(f) CC [2]: 40.36dB

1646  
1647  
1648  
1649  
1650  
1651  
1652  
1653  
1654  
1655  
1656  
1657  
1658

(g) WNNM-2 [10]: 41.24dB

(h) WNNM-3 [10]: 40.81dB

(i) MC-WNNM: 41.43dB

1659  
1660  
1661  
1662  
1663  
1664  
1665  
1666  
1667  
1668  
1669  
1670  
1671  
1672  
1673

(j) Mean Image [2]

Figure 12. Denoised images of a region cropped from the real noisy image “Nikon D800 ISO 1600 2” [2] by different methods. The images are better to be zoomed in on screen.

1674  
1675  
1676  
1677  
1678  
1679  
1680  
1681  
1682  
1683  
1684  
1685  
1686  
1687  
1688  
1689  
1690  
1691  
1692  
1693  
1694  
1695  
1696  
1697  
1698  
1699  
1700  
1701  
1702  
1703  
1704  
1705  
1706  
1707  
1708  
1709  
1710  
1711  
1712  
1713  
1714  
1715  
1716  
1717  
1718  
1719  
1720  
1721  
1722  
1723  
1724  
1725  
1726  
1727

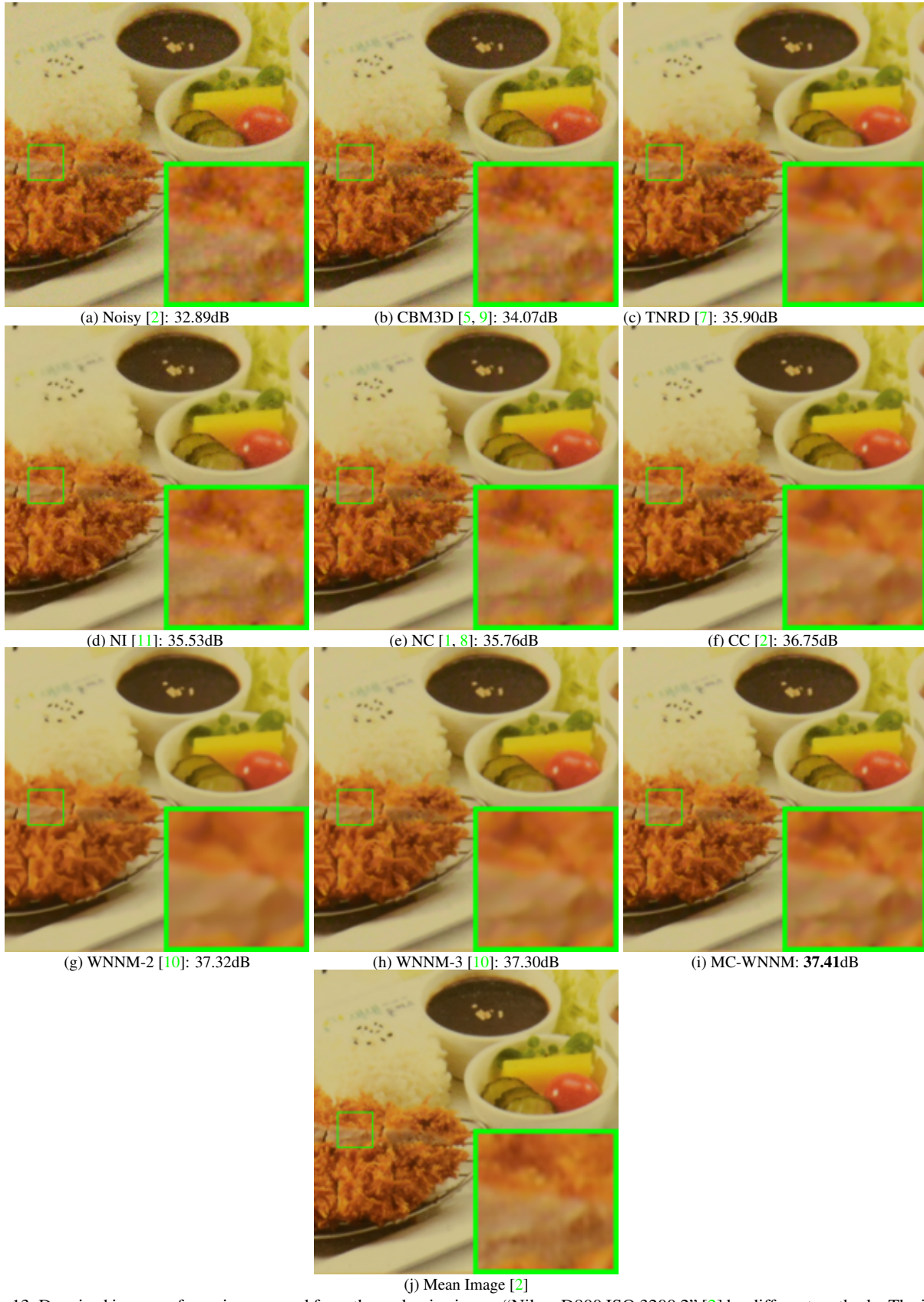


Figure 13. Denoised images of a region cropped from the real noisy image “Nikon D800 ISO 3200 2” [2] by different methods. The images are better to be zoomed in on screen.

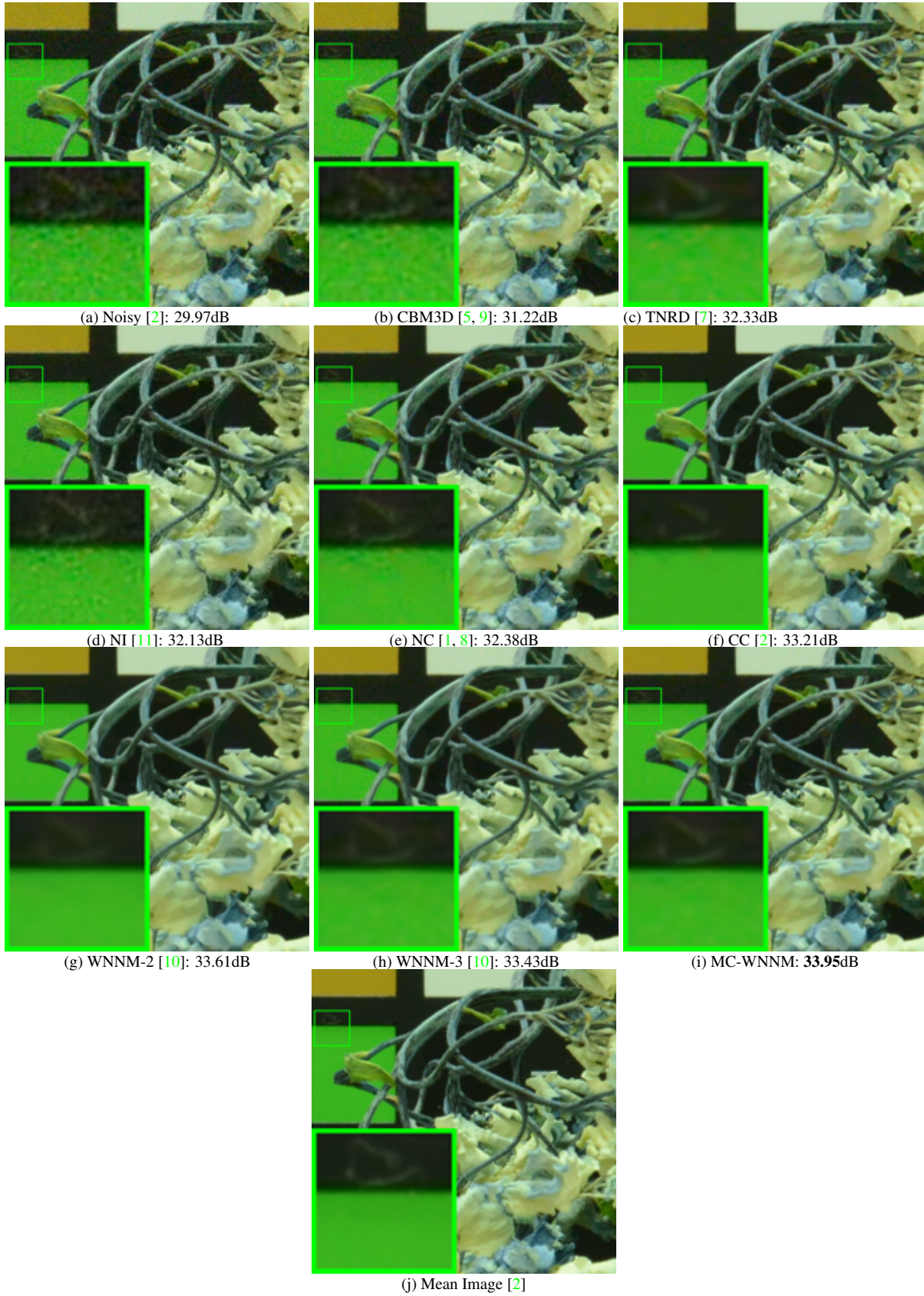


Figure 14. Denoised images of a region cropped from the real noisy image “Nikon D800 ISO 6400 2” [2] by different methods. The images are better to be zoomed in on screen.

1944 **References**

1998

- 1945 [1] M. Lebrun, M. Colom, and J. M. Morel. The noise clinic: a blind image denoising algorithm. [http://www.ipol.im/pub/  
art/2015/125/](http://www.ipol.im/pub/art/2015/125/). Accessed 01 28, 2015. 1, 4, 5, 6, 7, 8, 9, 10, 11, 12, 13, 14, 15, 16, 17, 18 1999
- 1946 [2] S. Nam, Y. Hwang, Y. Matsushita, and S. J. Kim. A holistic approach to cross-channel image noise modeling and its application to 2000 image denoising. *IEEE Conference on Computer Vision and Pattern Recognition (CVPR)*, pages 1683–1691, 2016. 1, 4, 15, 16, 17, 18 2001
- 1947 [3] C. Eckart and G. Young. The approximation of one matrix by another of lower rank. *Psychometrika*, 1(3):211–218, 1936. 1 2002
- 1948 [4] S. Gu, Q. Xie, D. Meng, W. Zuo, X. Feng, and L. Zhang. Weighted nuclear norm minimization and its applications to low level 2003 vision. *International Journal of Computer Vision*, pages 1–26, 2016. 1 2004
- 1949 [5] K. Dabov, A. Foi, V. Katkovnik, and K. Egiazarian. Color image denoising via sparse 3D collaborative filtering with grouping 2005 constraint in luminance-chrominance space. *IEEE International Conference on Image Processing (ICIP)*, pages 313–316, 2007. 5, 6, 7, 8, 9, 10, 11, 12, 13, 14, 15, 16, 17, 18 2006
- 1950 [6] H. C. Burger, C. J. Schuler, and S. Harmeling. Image denoising: Can plain neural networks compete with BM3D? *IEEE Conference 2007 on Computer Vision and Pattern Recognition (CVPR)*, pages 2392–2399, 2012. 5, 6, 7, 8, 9, 10, 11, 12, 13, 14 2008
- 1951 [7] Y. Chen, W. Yu, and T. Pock. On learning optimized reaction diffusion processes for effective image restoration. *IEEE Conference 2009 on Computer Vision and Pattern Recognition (CVPR)*, pages 5261–5269, 2015. 5, 6, 7, 8, 9, 10, 11, 12, 13, 14, 15, 16, 17, 18 2010
- 1952 [8] M. Lebrun, M. Colom, and J.-M. Morel. Multiscale image blind denoising. *IEEE Transactions on Image Processing*, 24(10):3149– 2011 3161, 2015. 5, 6, 7, 8, 9, 10, 11, 12, 13, 14, 15, 16, 17, 18 2012
- 1953 [9] K. Dabov, A. Foi, V. Katkovnik, and K. Egiazarian. Image denoising by sparse 3-D transform-domain collaborative filtering. *IEEE 2013 Transactions on Image Processing*, 16(8):2080–2095, 2007. 15, 16, 17, 18 2014
- 1954 [10] S. Gu, L. Zhang, W. Zuo, and X. Feng. Weighted nuclear norm minimization with application to image denoising. *IEEE Conference 2015 on Computer Vision and Pattern Recognition (CVPR)*, pages 2862–2869, 2014. 11, 12, 13, 14, 15, 16, 17, 18 2016
- 1955 [11] Neatlab ABSoft. Neat Image. <https://ni.neatvideo.com/home>. 11, 12, 13, 14, 15, 16, 17, 18 2017
- 1956 [12] 2018
- 1957 [13] 2019
- 1958 [14] 2020
- 1959 [15] 2021
- 1960 [16] 2022
- 1961 [17] 2023
- 1962 [18] 2024
- 1963 [19] 2025
- 1964 [20] 2026
- 1965 [21] 2027
- 1966 [22] 2028
- 1967 [23] 2029
- 1968 [24] 2030
- 1969 [25] 2031
- 1970 [26] 2032
- 1971 [27] 2033
- 1972 [28] 2034
- 1973 [29] 2035
- 1974 [30] 2036
- 1975 [31] 2037
- 1976 [32] 2038
- 1977 [33] 2039
- 1978 [34] 2040
- 1979 [35] 2041
- 1980 [36] 2042
- 1981 [37] 2043
- 1982 [38] 2044
- 1983 [39] 2045
- 1984 [40] 2046
- 1985 [41] 2047
- 1986 [42] 2048
- 1987 [43] 2049
- 1988 [44] 2050
- 1989 [45] 2051
- 1990 [46]
- 1991 [47]
- 1992 [48]
- 1993 [49]
- 1994 [50]
- 1995 [51]
- 1996 [52]
- 1997 [53]